Very Large Eddy Simulation of Draft Tube Flow

Walter GYLLENRAM Chalmers Univ. of Technology, Göteborg, Sweden gyllwalt@chalmers.se
Håkan NILSSON Chalmers Univ. of Technology, Göteborg, Sweden hani@chalmers.se

Key words: Turbulence, swirl, draft tube, vortex, filter, CFD.

Abstract

The objective of this work is to improve numerical predictions of unsteady turbulent flows in the draft tubes of hydraulic power plants. The standard two-equation turbulence models are known to have a strong damping effect on the resolved turbulence in this type of flow. In order to reduce this negative influence of the model, while retaining the usually satisfying near-wall behaviour, a dynamic filtering technique of the turbulent length and time scales is generalised, employed and evaluated. The filter limits the influence of the modeled turbulent length and time scales on the mean flow in regions where unsteadiness can potentially be resolved. The Wilcox (1988) $k-\omega$ turbulence model was chosen as basis for the investigations, and the effects of five different filter widths were examined. The original non-filtered model is also evaluated. A swirling flow through a straight axisymmetric diffuser was chosen as a test case and detailed measurements carried out by Clausen et al. were used to validate the numerical results. The influence of the filtering approach on the resolved frequencies and the time averaged solutions were analysed. It is shown that the filtering procedure gives better predictions of the time-averaged velocity field and more information on the large scale unsteadiness.

Introduction

There are many strategies for turbulence modeling for unsteady simulations, and Spalart (Ref 1) gave an overview and discussion about the advantages and limitations of these. As the Reynolds numbers of real water turbine flow are usually in the order of 10^7 or larger, large eddy simulation (LES) is not an option for a full scale simulation. On the other hand, traditional (statistical) turbulence models developed for the Reynolds (ensemble) averaged Navier-Stokes (RANS) equations can most often not distinguish between large and small scale turbulence or unsteadiness. This problem arises from the fact that most industrial closure models for the RANS equations are tuned for steady flow. In steady flow, the model must predict the influence of all turbulent time scales and, indirectly, all turbulent length scales as well. However, in a time resolved computation, there is a potential in resolving large turbulent time scales. There is obviously a need for a turbulence model that can distinguish between what can be resolved and what not. One method to accomplish this is to introduce a filtering procedure that limits the influence of the statistical turbulence model on the unsteady mean flow field. This is sometimes called very large eddy simulation (VLES) and there are many ways of formulating this filter. The filtering

approach in this work may in some sense be considered converse to the filtering approach that is used in LES. Instead of solving the filtered equations to avoid the computation of the small scales, the ensemble averaged turbulent length and time scales are filtered in order to allow their existence in the solution of the the mean flow field. This approach was initially developed by Willems (Ref 2) and is similar to the approach of Speziale (Ref 3, 4) and Fasel et al. (Ref 5), because the filter is applied directly to the Reynolds stress tensor and the turbulence model is left unchanged. To distinguish between large and small scale turbulence, the upper limit of the length scales of non-resolved turbulence is proportional to the local grid spacing or the product of the local velocity magnitude and the time step of the simulation. The latter constraint will only be active for large CFL numbers. There is no lower limit because the mean non-resolved turbulent length scale may be much smaller than the local grid spacing, especially close to walls. This will allow a much coarser grid resolution than in LES.

Turbulence modeling

The (1988) $k-\omega$ model of Wilcox (Ref 6) was investigated in the present work. The model is categorised as a two-equation eddy-viscosity model and is coupled to the averaged Navier-Stokes equations by the Boussinesq assumption,

$$-\overline{u_i' u_j'} = 2\nu_t S_{ij} - \frac{2}{3} k \delta_{ij}. \tag{1}$$

The Boussinesq assumption relates the Reynolds stress tensor to the mean strain rate tensor and introduces the concept of a turbulent eddy-viscosity, ν_t, where subscript t denotes *turbulence*. It suggests that the influence of turbulence on the mean flow is dominated by a mixing process, similar to molecular diffusion. The eddy-viscosity has the same dimension as the kinematic viscosity of the fluid and is assumed to be proportional to a function of the local turbulent length and time scales, i.e.

$$\nu_t \sim L_t^2 / T_t. \tag{2}$$

The length and time scales are local properties of the turbulent flow and must be modeled. A measure of the turbulent length and time scales can be obtained from dimensional analysis of the modeled turbulent kinetic energy, k, and dissipation rate, ε, or the specific dissipation rate, ω. The specific dissipation rate is defined as $\omega = \varepsilon/(\beta^* k)$. The constant of proportionality in Eq. (2) is usually called c_μ and, for most two-equation models, it obtains a value of 0.09, as does the model constant β^*.

Willems filtering approach

As mentioned in the introduction, there are various filtering approaches for unsteady CFD. As long as eddy-viscosity models are considered, the main issue is to determine which length and time scales should be used in the formulation of the eddy-viscosity. In this work, the filtering approach of Willems (Ref 2) was chosen as a basis. It was also used by Ruprecht et al. (Ref 7, 8) In contrast to the LES approach, where the filter is applied to the non-averaged Navier-Stokes equations in order to avoid the need for resolving the smallest turbulent scales, this filter is applied to the turbulence model in order to allow the existence of resolvable turbulent scales in the solution of the flow field. Willems derives the form of the filter function from the two-point correlation tensor and applies it to the modeled turbulent kinetic energy obtained from the $k-\varepsilon$ model. A derivation of the filter function based on dimensional analysis was made by Gyllenram (Ref 9). Gyllenram also showed that a generalisation of the filtering approach to other eddy-viscosity models than the $k-\varepsilon$ model requires that the filter is applied to the

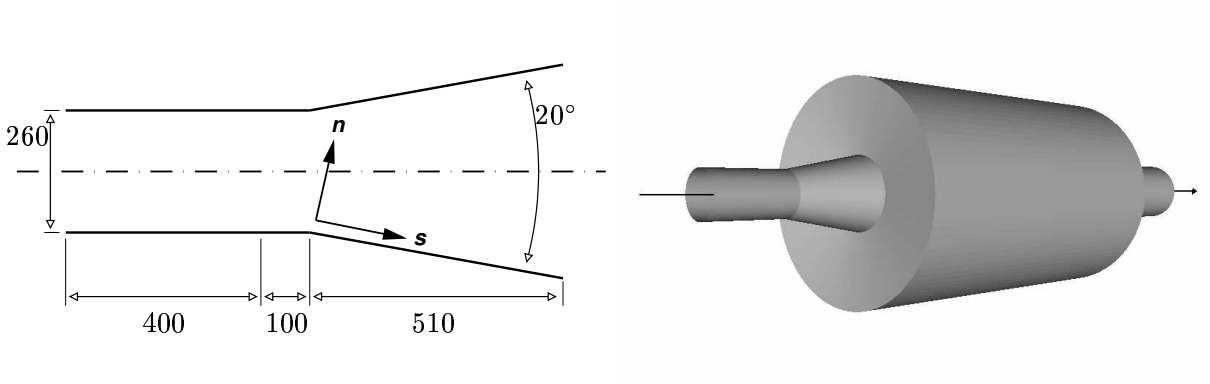

Figure 1 Left: The geometry of the testcase. All dimensions are in millimeters. The swirling flow enters from the left and the first 400 mm of the wall of the inlet straight pipe section is rotating. Right: The computational domain. The large dump downstream of the diffuser section is added to replace the open room that was used in the experiment.

turbulent length and time scales and not only to the turbulent kinetic energy, as in the work of Willems. If the filter is applied to the modeled turbulent length and and time scales of the flow, the filtered eddy-viscosity can be expressed as

$$\widehat{\nu}_t = g^2 \frac{k}{\omega}, \tag{3}$$

where the filter function $g(\ell_t, L_t)$ can be written

$$g = (\ell_t / L_t)^{2/3}, \tag{4}$$

and ℓ_t is defined as

$$\ell_t = \min\left\{L_t,\ \alpha \max\left\{|\mathbf{U}|\delta t,\ \Delta^{1/3}\right\}\right\}. \tag{5}$$

Coefficient $\alpha > 1$ takes into account the need for a limited number of cells to actually resolve a turbulent structure and Δ is the local cell volume. The computational time step may also set a lower limit to the resolved length scale because $|\mathbf{U}|\delta t$ is the shortest distance over which a fluid particle can be traced in an unsteady computation. A steady RANS calculation would correspond to an infinite time step and, for that case, it follows that $\ell_t = L_t$.

Test Case

A swirling flow through a straight conical diffuser was studied, see Fig. 1 (left). The diffuser has a half opening angle of 10° and exits to a large space. Upstream of the diffuser, there is a straight pipe section. Detailed measurements of the flow in this geometry were made by Clausen et al. (Ref 10), and the data are available in the ERCOFTAC database. The experimental data were sampled in the wall-normal direction at eight downstream positions in the tilted coordinate system shown in Fig. 1 (left). Directions n and s are referred to as the wall-normal and streamwise velocity, respectively. The three velocity components of this coordinate system will in the following be denoted $(V_n,\ V_\theta,\ V_s)$. The swirling component of the inlet flow was created in the experiment by a rotating honeycomb. The honeycomb section was 20 mm long and had a cell diameter of 3.2 mm. It was located 500 mm upstream of the expansion. Just downstream of the honeycomb, a screen was placed in order to reduce the boundary layer thickness. The wall of the inlet pipe section rotated at the same speed as the honeycomb until a point 100 mm upstream of the expansion. The boundary layer of the tangential velocity component will not

start to develop until this point is reached. The Reynolds number of the flow is $Re_D = 202,000$, and $V_\theta^{max}/U_b = 0.59$.

Computational considerations and boundary conditions

Swirling flows are generally more elliptic in nature than non-swirling flows. If a vortex rope is present, the oscillating pressure field will propagate upstream until it reaches a point at which it is forced to be symmetric. In this case the obvious point of forced symmetry is the location of the rotating honeycomb. At this position a near perfect solid body rotation was created. The screen that was located just downstream of the honeycomb, as well as the honeycomb itself, reduced the boundary layer thickness and created an axial velocity profile that was nearly constant in the radial direction (plug flow). Because of the well-defined instantaneous symmetric conditions at the position of the honeycomb, this is a good location for the inlet in an unsteady computation. In the experiment, the outlet of the diffuser was open to a large room. A large dump is added to the computational domain (see Fig. 1, right) in order to obtain similar outlet conditions of the diffuser in the numerical simulations, as well as to overcome the difficulties in prescribing a proper (unsteady) outlet boundary condition at this point. The dump will give the turbulent flow field a large degree of freedom similar to the opening to a large room. A pipe section is added at the end of the dump in order to accelerate the flow. Without this section, the velocities would be very low at the outlet, which could cause numerical problems. According to Andersson (Ref 11), the diameter and length of the dump should be at least three and five times the exit diameter of the diffuser, respectively. The flow can be expected to separate at the entrance of the outlet pipe section. In order to overcome the problem of recirculation at the outlet of the computational domain, this section should be long enough for the flow to reattach. In this case, the diameter of the outlet pipe section equals the outlet diameter of the diffuser. The length of the outlet pipe section is made three times the exit diameter of the diffuser.

The inlet boundary conditions for the velocity components were initially set as a solid body rotation for the tangential velocity profile ($V_\theta^{max}/U_b = 0.59$) and to a plug flow for the axial velocity component. The radial velocity component was set to zero. The axial inlet velocity profile was later reformulated as $V_z = U_b\left(V|_{z_0,\,r_0}/U_b + Cr^n\right)$ in order for the solution to better fit the data at the first measuring section, located 475 mm downstream of the inlet. The parameters are $C = \left(R^2\left(1 - V|_{z_0,\,r_0}/U_b\right)(n+2)\right)/(2R^{n+2})$, $n = 4$ and $V|_{z_0,\,r_0}/U_b = 0.98$, where U_b is the bulk velocity, z_0 and r_0 denote the axial location of the inlet and the centerline, respectively. A constant inlet turbulent intensity of 10% was chosen for all cases. A few studies of the impact of different values for the turbulent kinetic energy suggested that the absolute level of this variable at the inlet is of no significant importance for the solutions. The rotating honeycomb had a cell size of 3.2 mm. This was chosen as a measure for the inlet turbulent length scale, L_t, that is used in the definitions of the inlet boundary conditions for ω according to $\omega = \sqrt{k}/(\beta^* L_t)$.

Grids and code

Two different grids were considered for this work. In the following they will be referred to as grids A and B. Both grids are structured and axisymmetric. Grid A consists of $961,000$ nodes while grid B has $2,501,000$ nodes. Focusing on the most interesting part of the domain, i.e. the part that consists of the inlet pipe section and the diffuser, the number of cells in the different directions is $(N_r,\ N_\theta,\ N_z) = (31,\ 100,\ 124)$ for grid A and $(N_r,\ N_\theta,\ N_z) = (61,\ 100,\ 164)$ for grid B, with a wall-normal stretching of approximately 1.2 for grid A and 1.1 for grid

B. The computational domain was divided into ten equally sized blocks for efficient parallel computing. The CALC-PMB (Ref 12) CFD software was used for the calculations of this work. The code was developed at the Division of Fluid Dynamics, Department of Applied Mechanics, at Chalmers University of Technology, Göteborg. It is based on the finite volume method.

Results

The evolution of the streamwise and tangential velocity distributions can be seen in Fig. 2. The results are obtained using the Wilcox (1988) LRN $k-\omega$ turbulence model with different values of the filter coefficient, α, see Eq. (5). Grid A was used for these simulations. The computed flow field corresponds quite well to the experimental data, and it is clear that the filtering technique can improve the results. However, the results deteriorate if the filter width is too small. The filter coefficient, α, can be regarded as the number of cells that is needed to resolve a structure of the flow. If a very high value of the coefficient is chosen ($\alpha \to \infty$), the original non-filtered turbulence model will be recreated but all unsteady effects will vanish from the solution. For this test case, a choice of $(3 < \alpha < 4)$ improves the results significantly as compared to the non-filtered model. The mean velocity profiles correspond better to the

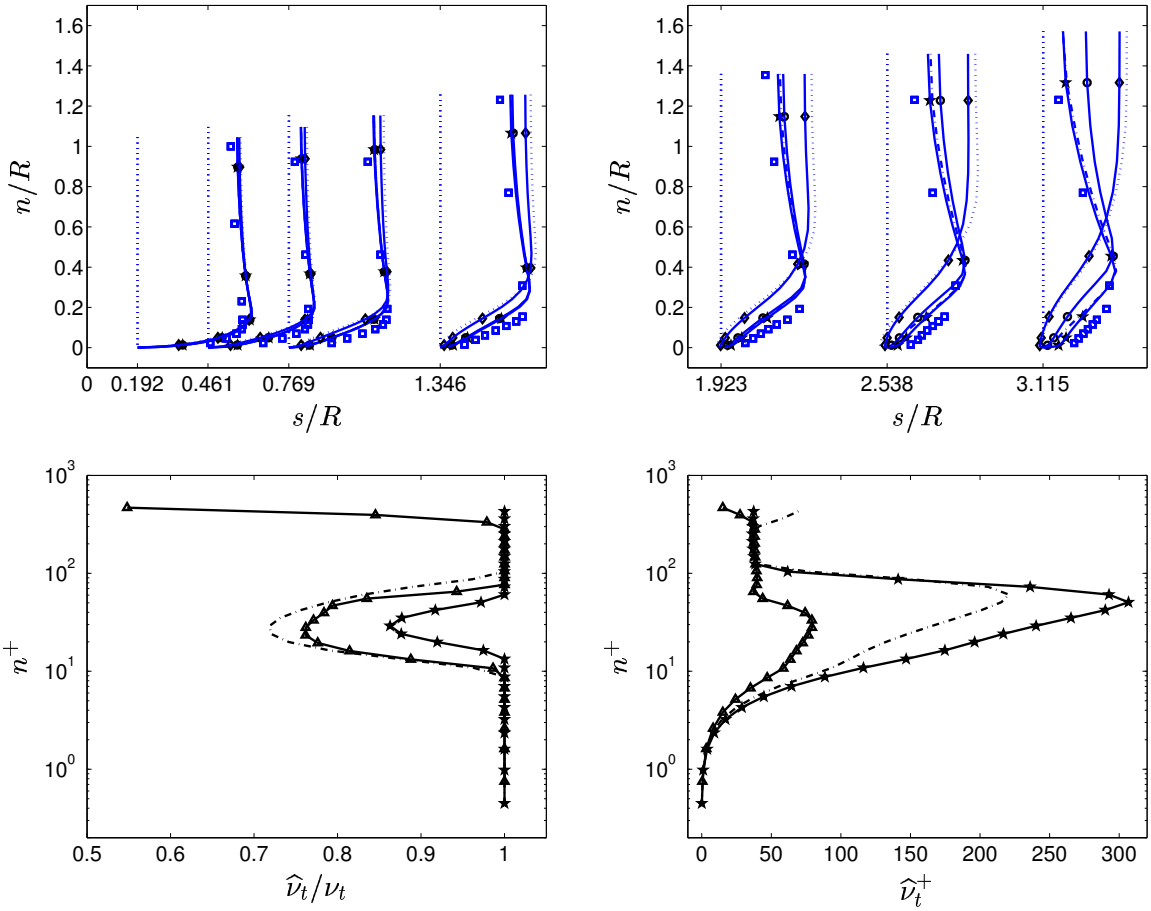

Figure 2 Top: Evolution of streamwise velocity. The different results are obtained by varying the filter width. [$\circ$]: $\alpha = \infty$. [$\star$]: $\alpha = 4$. [$\cdot-$]: $\alpha = 3$. [$\Diamond$]: $\alpha = 2.5$. [$\cdot\cdot$]: $\alpha = 2$. Bottom: Wall-normal distribution of the filter function (left) and $\widehat{\nu}_t^+$ (right) obtained from different filter widths and different grids. [$\cdot-$]: $\alpha = 3$, Grid A. [$\star$]: $\alpha = 4$, Grid A. [$\triangle$]: $\alpha = 3$, Grid B. The data are taken near the exit of the diffuser at $s/R = 3.115$. Only every second grid point is represented by a marker in the results from Grid B.

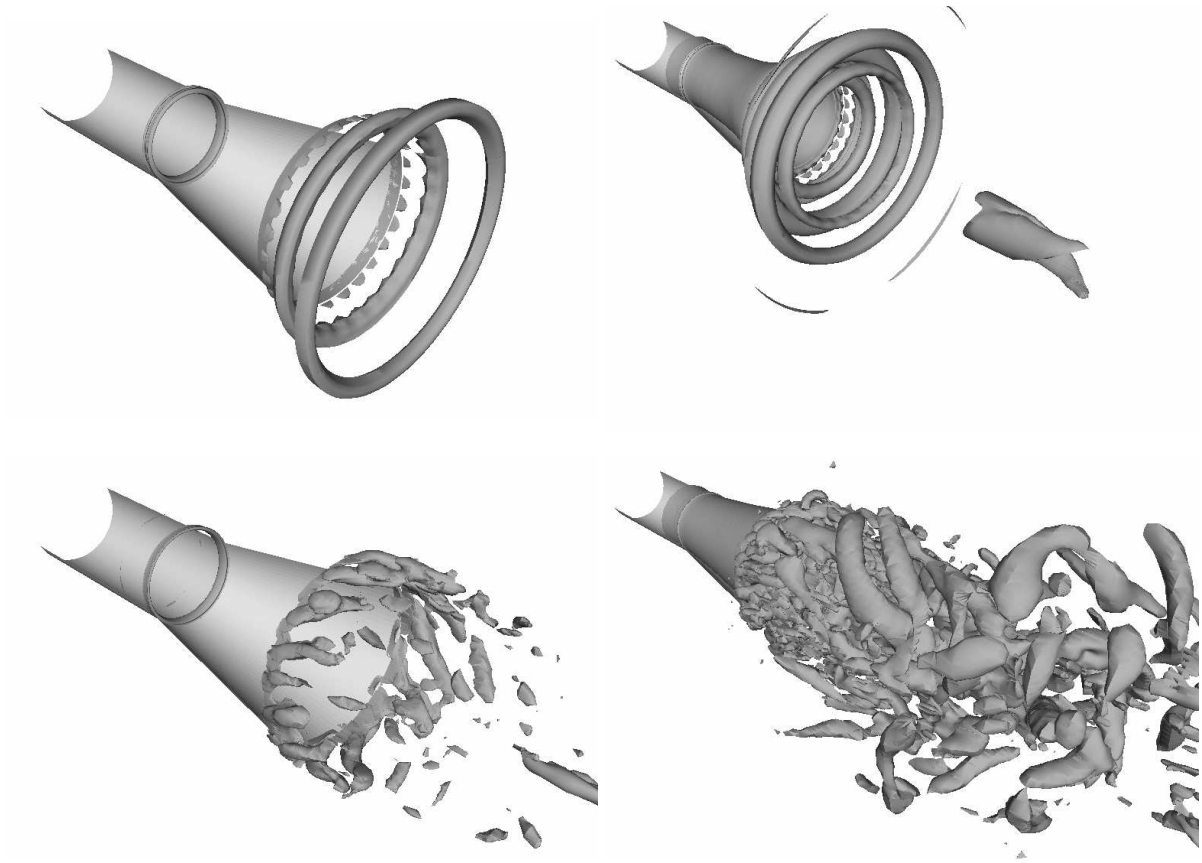

Figure 3 Positive iso-surfaces of the normalised second invariant of the velocity gradient tensor, $II_{\mathcal{V}}$. Top: Grid A, $\alpha = 3$, $II_{\mathcal{V}} = 0.5$ (left), $II_{\mathcal{V}} = 0.05$ (right). Bottom: Grid B, $\alpha = 3$, $II_{\mathcal{V}} = 0.5$ (left), $II_{\mathcal{V}} = 0.05$ (right). On the coarser grid, torus-shaped vortices that originate from the boundary layer of the diffuser are formed at the diffuser exit and interact with smaller, counter-rotating torus-shaped vortices. A fully turbulent flow field is obtained from the simulation on the finer grid.

measured data at the same time as large turbulent structures are resolved. However, the flow is obviously very sensitive to the choice of filter width, because a choice of $\alpha \leqslant 2.5$ leads to flow separation. The filter function and the eddy viscosity near the diffuser exit for the attached flow cases are shown in Fig. 2 (bottom). It is likely that too small a filter width makes the filter active all the way down to the viscous sublayer. This will cause the near wall behaviour of the model to deteriorate. Furthermore, too small a filter width introduces a gap between the filtered scales and what potentially can be resolved. This is not physically justified, and the results from these computations are obviously not trustworthy.

Instantaneous iso-surfaces of the normalised second invariant of the velocity gradient ($II_{\mathcal{V}}$) for the filtered $k - \omega$ model ($\alpha = 3$) are shown in Fig. 3 (top left). Using the coarse grid, large torus-shaped vortices are formed near the diffuser exit. Their radius grows as they are convected downstream. For the simulation using the non-filtered model (not shown), only two iso-surfaces (at the entrance and the exit of the diffuser section) of this value of $II_{\mathcal{V}}$ are visible, and are stationary. The effect of grid refinement on the simulations using the filtered model can be seen in Fig. 3 (bottom left). In this case, vortices that are more or less orthogonal to the flow direction are formed near the diffuser exit. They are distributed tangentially in a quite ordered manner. A look at smaller differences between the rotation rate and the strain rate tensors, i.e. $II_{\mathcal{V}} = 0.05$, yields even more information. Returning to the simulation using the filtered

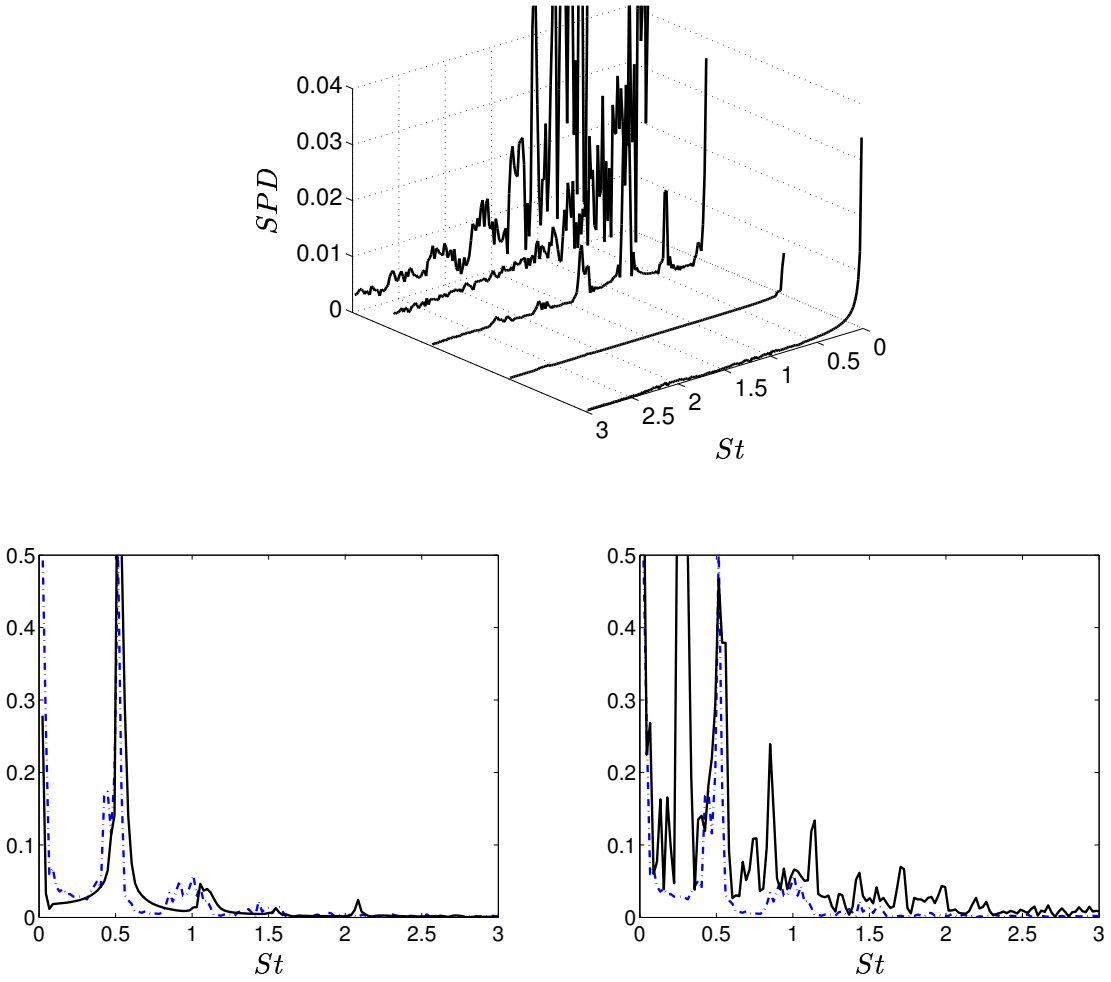

Figure 4 Top: Spectral power density of the wall pressure at $s/R = 3.115$ obtained from variation of the filter width for the Wilcox $k-\omega$ model on grid A. Left to right: $\alpha = \{2,\ 2.5,\ 3,\ 4,\ \infty\}$. The densities are based on 5,000 computational time steps, which equals 1.25 s of real time. Bottom left: Spectral power density of the wall pressure at the diffuser exit, variation of the filter width on grid A. [$\cdot-$]: $\alpha = 3$. [$-$]: $\alpha = 4$. Bottom right: Influence of grid resolution when using the same filter coefficient $\alpha = 3$. [$\cdot-$]: Grid A. [$-$]: Grid B. The latter figures are based on 4,000 computational time steps which equals 1 s of real time.

model on the coarser grid, we find that interesting things happen further downstream of the diffuser exit, see Fig. 3 (top right). The torus-shaped vortices that originate from the boundary layer of the diffuser also contain this value of II_Y, and they obviously interact with smaller counter-rotating vortices. Furthermore, a vortex shape reminiscent of a double helix is formed. A fully turbulent flow is obtained in the dump if a finer grid is used, see Fig. 3 (bottom right). This is a very good example of the strength of this approach: The method can dynamically switch between the mode in which all turbulence is modeled to the mode in which most of the turbulence is resolved.

Fourier transforms of the wall pressure were done to analyse the large scale unsteadiness of the flow in the diffuser. Fig. 4 (left) shows the spectral density of the wall pressure sampled at $s/R = 2.538$. The solutions obtained by using the filtered $k-\omega$ model with the filter width coefficient of $\alpha \leqslant 3$ especially shows a very high peak at $St = 0.85$. In this simulation, there

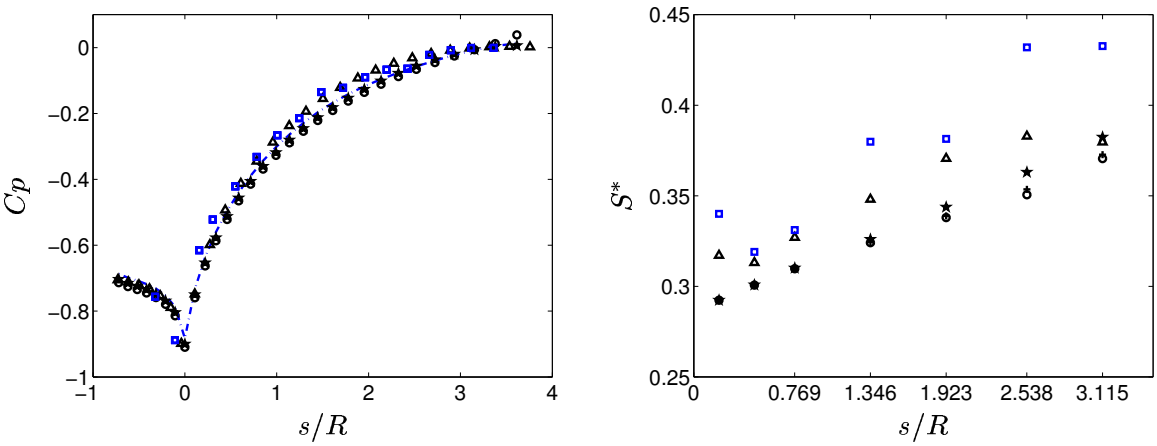

Figure 5 Non-dimensional wall pressure distribution $Cp = 2(P_{wall} - P_\infty)/(\rho U_b^2)$ (left) and evolution of swirl number (right). [$\circ$]: Wilcox $k-\omega$ model, Grid A. [$\cdot-$]: Filtered Wilcox $k-\omega$ model, $\alpha = 3$, Grid A. [$\star$]: Filtered Wilcox $k-\omega$ model, $\alpha = 4$, Grid A. [$\triangle$]: Filtered Wilcox $k-\omega$ model, $\alpha = 3$, Grid B. [$\square$]: Experiment.

are also two distinct overtones and one frequency of a magnitude that is half the dominant frequency. The spectral densities at the main frequencies in the simulation with $\alpha = 4$ are much lower at this point and, in the simulation using the non-filtered model, there are no distinct resolved frequencies whatsoever. For the last mentioned (non-filtered) simulation, there are also strong wiggles in the pressure field near the exit of the diffuser that contaminate the spectra. A comparison of the frequencies obtained from cases $\alpha = 3$ and $\alpha = 4$ at the very end of the diffuser (Fig. 4, center) shows that the spectral densities at the main frequencies are of the same magnitude at this point. The figure also suggests that the main frequencies of the solutions are not very sensitive to the choice of filter width. Neither does the resolution seem to play a major role in determining the main frequencies. Also shown in Fig. 4 (right) is the difference in frequency distribution from solutions obtained from grid A and grid B. The distinct peaks found in the simulation on grid A are also found when grid B is used. However, in the solution from the finer grid, there is an additional strong peak in the lower range, at approximately $St = 0.27$. The reason for this is not obvious. It is expected that a wider range of high frequencies would be resolved on the fine grid. This is indeed the case, as shown in Fig. 4 (right). The lower frequencies, on the other hand, are also expected to be found on the coarse grid. One explanation for this contradiction can be numerical errors. The lowest frequencies are the most difficult to predict accurately, as the numerical error in the time-dimension accumulates during the simulation.

The wall pressure distribution is shown in Fig. 5 (left). All calculations correspond quite well to the measured data. The largest deviations are found in the region around $s/R = 1.5$. However, the experimental results also show some scatter in this region. The choice of $\alpha = 4$ in Eq. (5) seems to lead to better predictions of the wall pressure in the inlet pipe section and near the exit of the diffuser. At this point, the slope of the wall pressure distribution almost vanishes. This agrees with experimental data. The result obtained when using the non-filtered model does not show this trend. When a swirling flow develops through a diffuser, the axial velocity will decelerate faster than the tangential velocity unless the rate of expansion of the diffuser is very small. This will create a relative increase in angular momentum as compared to the axial momentum, i.e. an increase in swirl number. As the axial velocity that is used in the definition of the swirl number is not measured, an approximate swirl number, $S^* = \int_0^N V_\theta V_s \, (N-n)^2 \, dn / (N \int_0^N V_s^2 \, (N-n) \, dn)$, where N is the normal distance from the wall

to the centerline, is used in this paper. This definition will give a slightly lower swirl number than the standard formulation. A standard midpoint quadrature method was used to integrate both the experimental and numerical data. In Fig. 5 (right), the evolution of swirl number S^* is shown. There is an almost linear relation between the streamwise (wall parallel, distance) and the swirl number. The computational results deviate about 10% from the experimental data. The predictions are somewhat improved when the filtered version of the $k-\omega$ model is used, and the results from the computations on the finer grid agree fairly well with the experiments. However, there are at least two sources of error in an integral quantity such as S^*. The numerical integration will cause errors in itself because of the different numbers of sampling points, which also are unevenly distributed radially. Second, the swirl number is extremely sensitive to the radial distribution of the axial velocity profile because of the square in the nominator. A better way to evaluate the results in Fig. 5 (right) is to look at the slope of the results, i.e. dS^*/ds, which describes the increase in swirl number. The computed results correspond very well to the experimental results in this aspect.

Conclusions

It has been shown that the results can be significantly improved by applying a spatial filtering technique to a two-equation LRN turbulence model. Without the filtering procedure, stationary solutions are obtained. The degree of unsteadiness in the resolved velocity field is obviously proportional to the filter width. However, too small a filter width may cause the results to deteriorate, and some caution must be used. If the filter is too small, there will be a spectral gap between the filtered scales and the scales that can potentially be resolved. Hence, too narrow a filter is not physically justified, and the results will not be trustworthy. Furthermore, it is preferable for the filter width to be large enough to enable the original asymptotic near-wall behaviour of the turbulence model. Nevertheless, it should be small enough to allow the resolution of large scale unsteadiness away from walls. A filter width of approximately three to four times the third root of the local computational cell volume seems in the present study to be optimal. The positive effects of introducing the filtering technique to the present test case most likely owe to a more accurate prediction of the complicated flow field at the exit of the diffuser. This region is dominated by a highly unsteady vortex breakdown with secondary flow structures that are not accurately predicted when the original (non-filtered) model is employed. However, as there is a potential in resolving these large scale structures in an unsteady simulation, the filtering technique can be successfully applied. The length scale of the local grid spacing appears explicitly in the filter function, and it is expected that the instantantaneous solution is influenced by grid refinement. A study of the influence of the grid resolution shows that the grid dependence cannot be neglected in this case. However, it is impossible to say without further study whether this is due to the filtering procedure or to numerical problems at the critical regions of the flow. The critical regions are the endpoint of the rotating wall, the entrance of the diffuser section and the exit of the diffuser. Further studies in which these regions are better resolved, especially in the axial direction, must be made. In particular, the axial resolution seems to be important.

The main frequencies of the unsteadiness seem to be quite independent of both the filter size and the grid resolution. Moreover, the amplitudes are of the same order, at least near the diffuser exit.

Acknowledgements
The research presented in this paper has been part of the "Water turbine collaborative R&D program" which is financed by the Swedish Energy Agency, Hydro Power companies[1] (through Elforsk AB), GE Energy (Sweden) AB and Waplans Mekaniska Verkstad AB. Much of the computational work was carried out under the HPC-EUROPA project (RII3-CT-2003-506079), with the support of the European Community - Research Infrastructure Action under the FP6 "Structuring the European research area" Program. The authors would also like to thank Dr. Ruprecht at IHS, University of Stuttgart, for support during this work.

References

Ref 1 P. R. Spalart. Strategies for turbulence modeling and simulations. *Int. J. Heat and Fluid Flow*, 21:252–263, 2000.

Ref 2 W. Willems. *Numerische Simulation turbulenter Scherströmungen mit enem Zwei-Skalen Turbulenzmodell*. Thesis for the degree of Doctor of Philosophy, Rheinish-Westfälischen Technischen Hochschule, Aachen, Germany, 1996.

Ref 3 C. G. Speziale. Turbulence modeling for time-dependent RANS and VLES: A review. *AIAA Journal*, 36:173–184, 1998.

Ref 4 C. G. Speziale. A combined large-eddy simulation and time-dependent RANS capability for high-speed compressible flows. *J. Scientific Computing*, 13(3):253–274, 1998.

Ref 5 H. F. Fasel, J. Seidel, and S. Wernz. A methodology for simulations of complex turbulent flows. *J. Fluids Engineering*, 124:933–942, 2002.

Ref 6 D.C. Wilcox. Reassessment of the scale-determining equation for advanced turbulence models. *AIAA J.*, 26(11):1299–1310, 1988.

Ref 7 A. Ruprecht et. al. Massively parallel computation of the flow in hydro turbines. In *Proceedings of the XXIst IAHR Symposium*, volume 1, pages 199 – 206, 2002.

Ref 8 A. Ruprecht, T. Helmrich, T. Aschenbrenner, and T. Scherer. Simulation of vortex rope in a turbine draft tube. In *Proceedings of the XXIst IAHR Symposium*, volume 1, pages 259 – 265, 2002.

Ref 9 W. Gyllenram. *Analytical and Numerical Investigations of Steady and Unsteady Turbulent Swirling Flow in Diffusers*. Thesis for the degree of Licentiate of Engineering, no. 2006:05, ISSN 1652-8565, Chalmers University of Technology, Göteborg, Sweden, 2006.

Ref 10 P. D. Clausen, S. G. Koh, and D. H. Wood. Measurements of a swirling turbulent boundary layer developing in a conical diffuser. *Experimental Thermal and Fluid Science*, 6:39–48, 1993.

Ref 11 K. Andersson. Personal communication, Siemens Industrial Turbomachinery AB, Finspång, Sweden, 2005.

Ref 12 H. Nilsson. *Numerical Investigations of Turbulent Flow in Water Turbines*. Thesis for the degree of Doctor of Philosophy, ISBN 91-7291-187-5, Chalmers University of Technology, Göteborg, Sweden, 2002.

[1] Vattenfall AB Vattenkraft, Fortum Generation AB, Sydkraft Vattenkraft AB, Skellefteå Kraft AB, Graninge Kraft AB, Jämtkraft AB, Sollefteåforsens AB, Karlstads Energi AB, Gävle Energi AB, Öresundskraft AB